nature climate change

LETTERS

PUBLISHED ONLINE: 14 NOVEMBER 2016 | DOI: 10.1038/NCLIMATE3157

A re-examination of the projected subtropical precipitation decline

Jie He[1]* and Brian J. Soden[2]

A large-scale precipitation decline in the subtropics is a widely accepted projection of future climate change[1–3], but its causes and implications are uncertain. Two mechanisms are commonly used to explain the large-scale subtropical precipitation decline: an amplification of moisture export due to the increase in moisture[4] and a poleward shift of subtropical subsidence associated with the poleward expansion of the Hadley cell[5,6]. In an idealized experiment with abrupt CO_2 increase, we find that the subtropical precipitation decline forms primarily in the fast adjustment to CO_2 forcing during which neither of the two proposed mechanisms exists. Permitting the increase in moisture and the Hadley cell expansion does not substantially change the characteristics of the large-scale subtropical precipitation decline. This precipitation change should be interpreted as a response to the land–sea warming contrast, the direct radiative forcing of CO_2 and, in certain regions, the pattern of SST changes. Moreover, the subtropical precipitation decline is projected predominately over oceans. Over subtropical land regions, the precipitation decline is muted or even reversed by the land–sea warming contrast.

The subtropics encompass many of the world's driest regions and climate models consistently predict a large-scale decline in subtropical precipitation from anthropogenic forcing[1–3]. The subtropical precipitation decline (SPD) has been commonly related to the 'dry-get-drier' paradigm, which was articulated in the influential work of Held and Soden to explain changes in the hydrological cycle (precipitation minus evaporation, hereafter P–E)[4]: as the Earth gets warmer, the increasing moisture amplifies the existing pattern of (P–E). Held and Soden suggested that because changes in precipitation have considerably more spatial structure than changes in evaporation, much of the decline in subtropical P–E should be associated with a decline in precipitation.

Although the 'dry-get-drier' mechanism has proved an effective first-order explanation for the large-scale changes in P–E, some studies questioned whether it fully explains the SPD[5,6]. These studies argued that the SPD is primarily driven by a poleward shift of subsidence associated with the expansion of the Hadley cell. Despite their disagreement, both the 'dry-get-drier' and poleward expansion mechanisms successfully predict the SPD, particularly from a zonal mean perspective. However, it is unclear whether these theories are consistent with model simulations at regional scales.

Here, an examination of the spatial patterns of the projected precipitation change shows that the robust SPD occurs primarily over oceanic regions, but rarely over subtropical land (Table 1, top row). Compared with the common expectation that the subtropics will generally receive less rainfall[3,7,8], the lack of large-scale decline over subtropical land has been less appreciated and is not expected by either of the previously proposed mechanisms. Indeed, it has been noted that the hydrological changes over land do not follow the 'dry-get-drier' paradigm[9–11]. This study aims to evaluate and understand the mechanisms of the projected SPD with a focus on its land–sea distribution.

In a global warming scenario, the external radiative forcing and the surface warming drive changes in the atmosphere. A common characteristic of the 'dry-get-drier' and the poleward expansion mechanisms is that they are both predominantly driven by the global mean sea surface temperature (SST) warming[12–14]. Therefore, if the SPD is caused by the 'dry-get-drier' or poleward expansion mechanism, it must follow the rate of increase in SST. On the other hand, precipitation changes can also be directly driven by the increasing CO_2 independently of the warming. In particular, it has been found that a large portion of the tropical precipitation changes result from the reduced atmospheric radiative cooling associated with the direct forcing of CO_2 (ref. 15). However, the relative roles of these mechanisms in driving the SPD remain unclear.

To understand the mechanisms of the SPD, we first analyse an ensemble of 13 model simulations, in which the CO_2 concentration is abruptly quadrupled and held constant for 150 years (abrupt4×CO_2, Methods). In the abrupt4×CO_2 simulation, the global mean SST slowly increases and eventually reaches a perturbation of about 4K. During the first year of the simulation, there is little global mean SST warming, nor is there substantial increase in moisture or poleward expansion of the Hadley cell (Fig. 1a,c). However, precipitation shows a rapid decline in most subtropical regions (Fig. 1e). Both the amplitude and pattern of the fast precipitation decline are similar to those at the end of the simulation (Fig. 1f; extended analysis in Supplementary Section 2).

The temporal inconsistency between the SPD and the two previously proposed mechanisms is also evident from Fig. 2. The 'dry-get-drier' and poleward expansion mechanisms develop over time. Although the latter matures faster[16,17], both are relatively weak at the beginning of the simulation. On the other hand, the SPD forms immediately after the CO_2 quadrupling. It appears that the initial zonal mean decline in the Southern Hemisphere largely persists over time, whereas the Northern Hemisphere decline is more transient, mainly due to the slow moistening in the subtropical northwest Pacific and the east coast of the United States (Fig. 1f). The fact that the SPD is primarily a fast response to the abrupt CO_2 forcing indicates that the 'dry-get-drier' and poleward expansion mechanisms are not the main cause. In contrast to the fast SPD, the extratropical precipitation increases rather slowly, consistent with a thermodynamic response[4].

To further demonstrate the cause of the SPD, we analyse a more realistic emission scenario, in which CO_2 increases by 1% per year for 140 years (1pctCO_2, Methods). We calculate precipitation change as the difference between the first and last

[1]Princeton University, and NOAA/Geophysical Fluid Dynamics Laboratory, Princeton, New Jersey 08540, USA. [2]Rosenstiel School of Marine and Atmospheric Science, University of Miami, Miami, Florida 33149, USA. *e-mail: Jie.He@noaa.gov

Table 1 | Area fraction of robust subtropical precipitation change.

	Land percentage of robust $-\delta P$	Land percentage of robust $+\delta P$	Percentage of land with robust $-\delta P$	Percentage of land with robust $+\delta P$
1pctCO_2	16.5	32.7	11.0	26.1
AMIP(total)	14.9	30.3	11.8	24.4
AMIP(total) − AMIP_CO_2(dyn)	26.3	17.1	18.1	13.7

The left two columns are the area fraction of the robust subtropical precipitation decline (increase) that is projected over land. The right two columns are the area fraction of subtropical land that projects robust negative (positive) precipitation change. Robustness is defined in the Methods. The subtropics are defined between 10° and 50° latitude in both hemispheres. Results (top to bottom) are from the 1pctCO_2 simulation, sum of the three AMIP simulations (AMIP_CO_2, AMIP_mean and AMIP_pattern) and sum of the three AMIP simulations with the dynamic precipitation change from AMIP_CO_2 subtracted. Note that 26.9% of the subtropics is covered with land. Refer to Supplementary Section 1 for analyses of individual models.

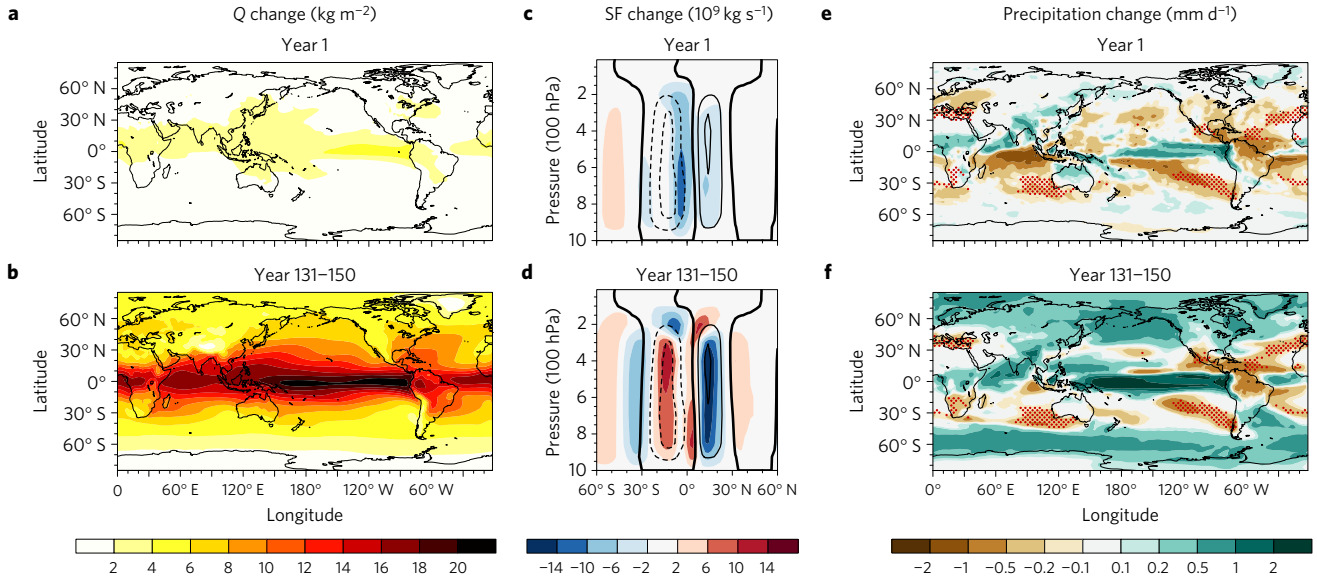

Figure 1 | Multi-model ensemble mean changes in the abrupt4×CO_2 simulation. Shading of the left, middle and right columns shows changes in the vertically integrated water vapour, changes in the zonal mean stream function and changes in precipitation, respectively. **a**–**f**, Changes in the first year (**a**,**c**,**e**) and the average change of the last 20 years (**b**,**d**,**f**). Red stippling in the right column indicates regions of robust SPD defined with the precipitation change of years 131–150 (Methods). Contours in the middle column show the climatology of the zonal mean stream function with an interval of 4×10^{10} kg s^{-1}. Zero contours are thickened. Dashed contours indicate negative values. The poleward expansion of the Hadley cell is evident in **d** as subsidence is strengthened near the 30° latitude, pushing the zero climatology contour poleward in both hemispheres.

20 years of the simulation (Fig. 3a). To separate the 'dry-get-drier' and poleward expansion mechanisms from other factors, we use three sets of atmosphere-only (AMIP) simulations in which the increase in CO_2, the global mean SST warming and the pattern of SST change are specified separately (Methods). We refer to them as AMIP_CO_2, AMIP_mean and AMIP_pattern, respectively. Note that the increase in moisture and the Hadley cell expansion predominately exist in the AMIP_mean simulation and are inappreciable in the other two AMIP simulations[14].

Overall, the SPD in the 1pctCO_2 simulation is well reproduced by the sum of AMIP_CO_2, AMIP_mean and AMIP_pattern (Fig. 3a,b, red stippled area), lending credence to our approach. As shown in Fig. 3d, the AMIP_CO_2 simulation clearly dominates the large-scale SPD. The pattern of SST change substantially decreases precipitation over the southeast Pacific and the northwest Atlantic as a result of the reduced local SST warming[18], but has little impact in the other regions of SPD[19] (Fig. 3f).

As shown in Fig. 3e, the AMIP_mean simulation exhibits a 'wet-get-wetter' response, with increased precipitation over most regions of positive climatological P–E. In comparison, however, there is a general lack of the 'dry-get-drier' counterpart, except in the southern Indian Ocean and the Mediterranean regions. Although the mean SST warming does not drive the large-scale SPD, it dominates the decrease in subtropical P–E over ocean (Supplementary Section 3), consistent with the intensified subtropical moisture export associated with warming[4,20]. In Fig. 4, we analyse the moisture budget in the SPD regions (Methods). As shown in the 'AMIP_mean' column, the warming of SST amplifies the moisture export; however, it also increases evaporation, which completely balances out the 'dry-get-drier' mechanism. Therefore, although the subtropical moisture export intensifies with warming, there is no net moisture deficiency that would require a decrease in precipitation.

As indicated by the dark blue bars in Fig. 4, the total contribution of the mean SST warming to precipitation changes in the SPD regions is slightly positive (which opposes the decline). The AMIP_CO_2 simulation reproduces most of the subtropical precipitation decline, followed by the AMIP_pattern simulation. These results further disprove the 'dry-get-drier' and poleward expansion mechanisms as the main cause of the SPD.

Next, we discuss the mechanisms that drive the SPD in the AMIP_CO_2 simulation. Because land is free to warm in this simulation (Methods), the changes in precipitation are driven not only by the direct radiative forcing of CO_2 but also by the contrast in the rate of warming between land and sea. The land–sea warming contrast in the AMIP_CO_2 simulation has a similar amplitude to that in the fast response to abrupt CO_2 quadrupling (Supplementary Section 2). Previous studies of the tropics showed that the direct radiative forcing of CO_2 stabilizes the atmosphere and weakens convection[14,15], whereas the land–sea warming contrast shifts convection from ocean to land[14,21,22]. However,

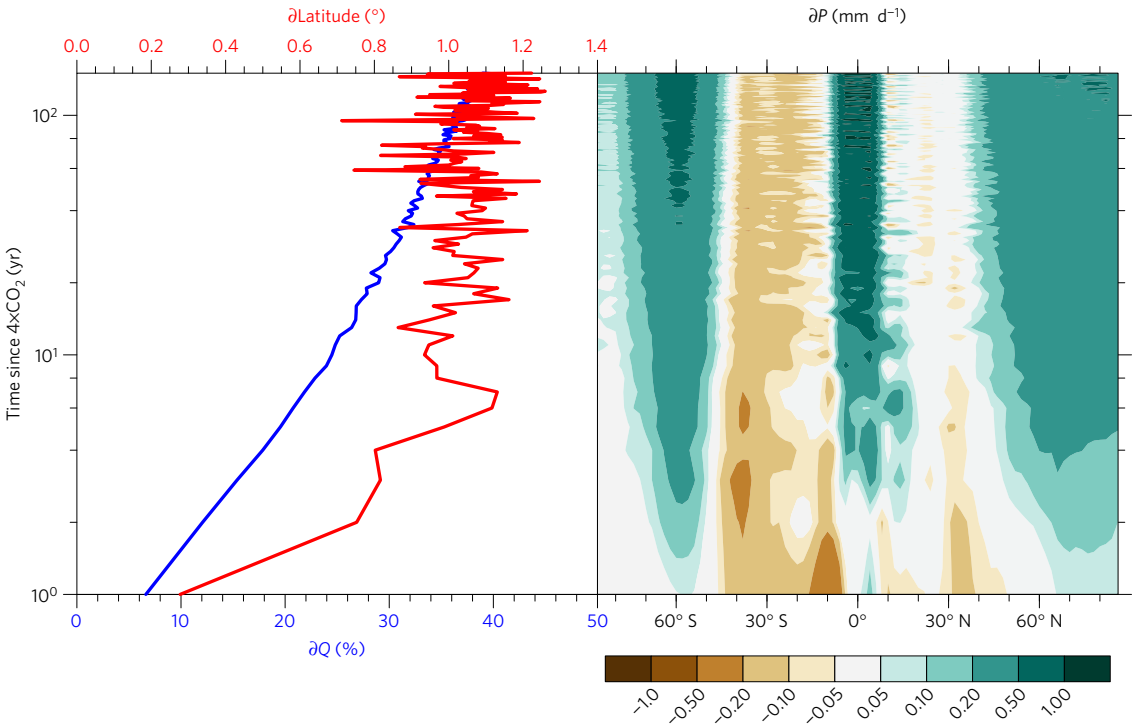

Figure 2 | Time evolution of multi-model ensemble mean changes in the global mean moisture, boundary of the Hadley cell and zonal mean precipitation from the abrupt4 x CO_2 simulation. Changes in moisture (left blue line) are integrated vertically and globally and presented as percentage changes. The boundary of the Hadley cell is defined as the point of zero zonal mean stream function at 500 hPa between 20° and 40° latitude. Changes in the Hadley cell boundary (left red line) are averaged between the two hemispheres. Zonal mean precipitation changes are shown in the right panel. The time (y) axis is logarithmically spaced.

the relative importance of the two mechanisms for the SPD is unclear.

To understand the roles of the direct CO_2 forcing and land–sea warming contrast, we analyse the subtropical precipitation changes in the aquaplanet simulation with increasing CO_2 and fixed SST (aqua_CO_2, Methods). The aqua_CO_2 simulation has the same direct CO_2 forcing as that from AMIP_CO_2, but does not contain land–sea warming contrast. Although the longitudinal climatology of the aquaplanet simulation differs from that of the AMIP simulations, it reasonably reproduces the zonal mean climatology and the latitudinal positions of SPD (Supplementary Section 4).

As shown in Fig. 4, the aqua_CO_2 simulation also projects a SPD albeit with smaller magnitude compared with the AMIP_CO_2 simulation, indicating that the direct radiative forcing of CO_2 indeed contributes to the development of the SPD. The SPD in the AMIP_CO_2 simulation is primarily associated with a decrease in evaporation and a dynamic precipitation decline (due to changes in circulation, Methods). The former is reproduced by the aqua_CO_2 simulation, whereas the latter is not. (Refer to Supplementary Section 5 for a comparison of the AMIP and aquaplanet simulations using the same set of models, which yields almost identical results.) This indicates that the dynamic precipitation change from the AMIP_CO_2 simulation is most likely caused by the land–sea warming contrast.

In addition, the dynamic precipitation reductions in the AMIP_CO_2 simulation occur primarily over ocean and are accompanied by the dynamic increases over land (Supplementary Fig. 4S). Such a pattern of precipitation response further supports the land–sea contrast mechanism, since CO_2 increases uniformly in space and should not discriminate land from ocean. As shown in Supplementary Section 6, the land precipitation increase generally occurs in the summer hemisphere and appears to be associated with an enhancement of the existing summer monsoon circulations. On the other hand, the oceanic precipitation reduction is likely to result from a combination of a monsoon-like surface circulation response and an intensification of the subtropical anticyclone over ocean through the propagation of Rossby waves[23].

Because most of the SPD regions are located over ocean (Fig. 3a,b), an ocean-to-land shift of precipitation enhances the development of the SPD. On the other hand, such a shift also acts to prevent a SPD over land. As shown in Table 1, the coupled models project SPD over only a small fraction of subtropical land. However, if the dynamic precipitation change from the AMIP_CO_2 simulation is subtracted from the total precipitation change, models would project a substantially larger area of land decline (Table 1, bottom row), including central North Africa, the Middle East, southeast Africa and east Australia (Fig. 3c). This hypothetical SPD over land would be primarily driven by the SST warming (Fig. 3e), possibly through the increased tropospheric stability associated with the enhanced convection over ocean[14,24,25].

We have shown that the SPD is largely a dynamic response and unrelated to the 'dry-get-drier' paradigm. The dynamic precipitation decline was previously associated with the poleward expansion of the zonal mean subsidence due the positional match between the two[5,6]. Mechanistically, however, it is primarily a land–sea shift driven by the land–sea warming contrast, which strengthens the subtropical subsidence over ocean while weakening it over land, yielding little zonal mean change[14]. In an idealized experiment of abrupt CO_2 forcing, the SPD develops instantaneously, much faster than the moisture increase and the Hadley cell expansion. Observations of the recent decades suggest that a large-scale SPD could already be underway[2]. The fact that the SPD is predominantly a fast response implies that the subtropics may have already realized most of the precipitation decline that would result from current radiative forcing levels.

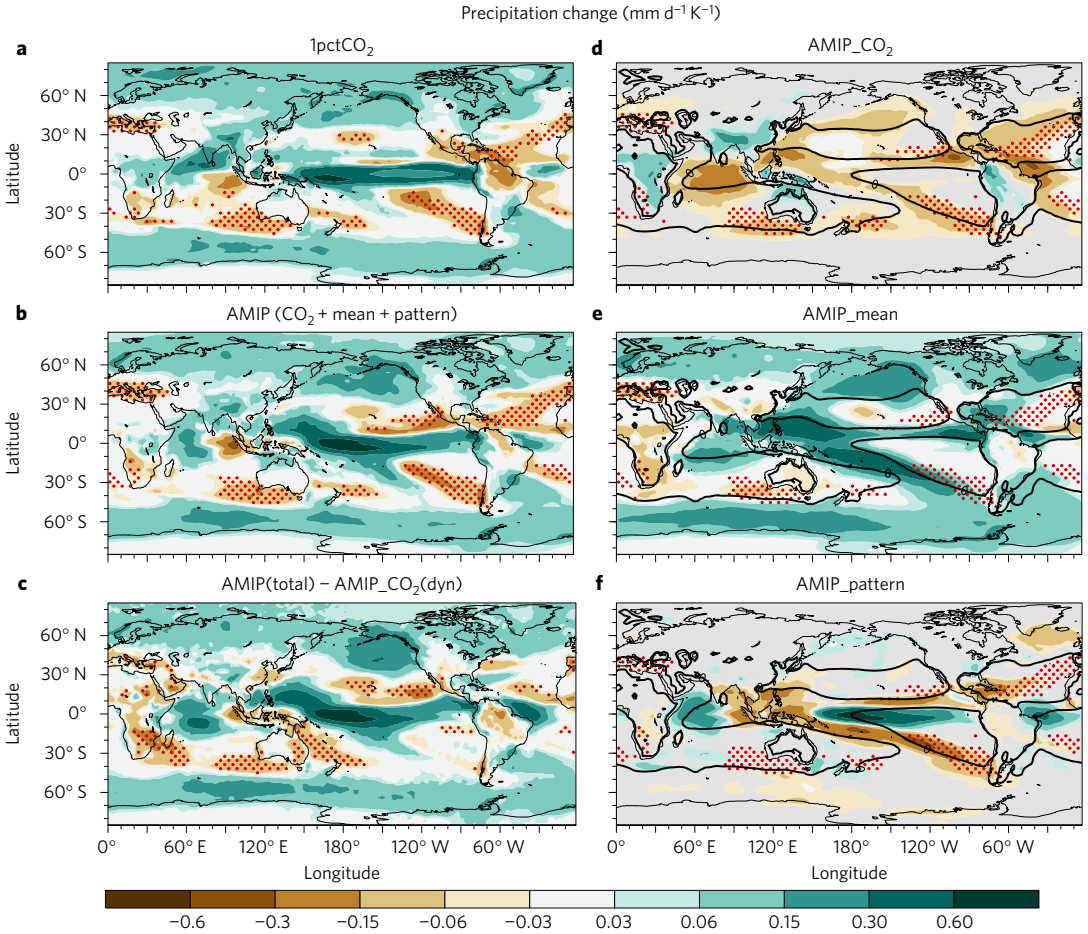

Figure 3 | Multi-model ensemble mean precipitation changes. a,**b**, Changes from the 1pctCO$_2$ simulation (**a**) and sum of the three AMIP simulations (**b**). **c**, Changes from the sum of the three AMIP simulations but with the dynamic precipitation change from the AMIP_CO$_2$ simulation removed. **d**–**f**, Changes from the AMIP_CO$_2$ simulation (**d**), the AMIP_mean simulation (**e**) and the AMIP_pattern simulation (**f**). Zero contours of climatological P–E are shown in **d**–**f**. The red stippling in **a**–**c** marks regions of robust SPD (Methods) of the respective simulations. The red stippling in **d**–**f** marks the robust SPD regions of the sum of the AMIP simulations and is the same as that in **b**.

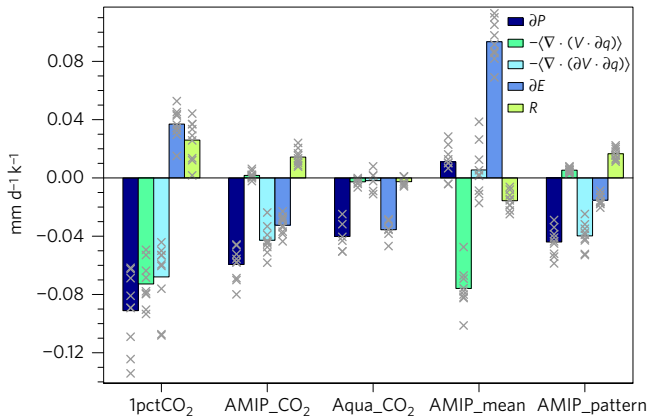

Figure 4 | Changes in the moisture budget terms for the robust SPD regions from the 1pctCO$_2$, AMIP and aqua_CO$_2$ simulations. Bars are the ensemble mean changes, whereas crosses are changes from each individual model. The robust SPD regions are defined in the Methods. For the AMIP_CO$_2$, AMIP_mean and AMIP_pattern simulations, the terms are calculated over the robust SPD regions in the sum of the three AMIP simulations, as indicated by the red stippling in Fig. 3d–f. Note that the aquaplanet simulation uses a partially different set of models (Methods); refer to Supplementary Section 5 for a comparison using the same set of models.

Despite the expected large-scale SPD, climate models do not project a robust decline over subtropical land. This could be in part due to the greater challenge in modelling hydrological processes over land. However, models consistently show that the enhanced land warming and associated circulation change largely offsets the land precipitation decline driven by the warming of SST (Supplementary Section 1). As a result, the SPD is projected over only a small fraction of subtropical land regions, including southwest Africa, the coast of the Mediterranean Sea and the southern part of Chile (Fig. 3a). In these regions, the precipitation decline is primarily driven by the slow warming of the global mean SST (Fig. 3 and Supplementary Section 5) and may continue to develop long after the greenhouse gas concentrations stop rising[26].

Methods

Methods and any associated references are available in the online version of the paper.

Received 4 July 2016; accepted 13 October 2016; published online 14 November 2016

References

1. Allen, M. R. & Ingram, W. J. Constraints on future changes in climate and the hydrologic cycle. *Nature* **419,** 224–232 (2002).
2. Neelin, J. D., Münnich, M., Su, H., Meyerson, J. E. & Holloway, C. E. Tropical drying trends in global warming models and observations. *Proc. Natl Acad. Sci. USA* **103,** 6110–6115 (2006).

3. IPCC *Climate Change 2007: The Physical Science Basis* (eds Solomon, S. *et al*.) (Cambridge Univ. Press, 2007).
4. Held, I. M. & Soden, B. J. Robust responses of the hydrological cycle to global warming. *J. Clim.* **19,** 5686–5699 (2006).
5. Scheff, J. & Frierson, D. Twenty-first-century multimodel subtropical precipitation declines are mostly midlatitude shifts. *J. Clim.* **25,** 4330–4347 (2012).
6. Scheff, J. & Frierson, D. M. W. Robust future precipitation declines in CMIP5 largely reflect the poleward expansion of model subtropical dry zones. *Geophys. Res. Lett.* **39,** L18704 (2012).
7. Seager, R. *et al*. Model projections of an imminent transition to a more arid climate in southwestern North America. *Science* **316,** 1181–1184 (2007).
8. Hansen, J. *et al*. Target atmospheric CO_2: where should humanity aim? *Open Atmos. Sci. J.* **2,** 217–231 (2008).
9. Greve, P. *et al*. Global assessment of trends in wetting and drying over land. *Nat. Geosci.* **7,** 716–721 (2014).
10. Roderick, M. L., Sun, F., Lim, W. H. & Farquhar, G. D. A general framework for understanding the response of the water cycle to global warming over land and ocean. *Hydrol. Earth Syst. Sci.* **18,** 1575–1589 (2014).
11. Byrne, M. P. & O'Gorman, P. A. The response of precipitation minus evapotranspiration to climate warming: why the 'wet-get-wetter, dry-get-drier' scaling does not hold over land. *J. Clim.* **28,** 8078–8092 (2015).
12. Frierson, D. M. W., Lu, J. & Chen, G. Width of the Hadley cell in simple and comprehensive general circulation models. *Geophys. Res. Lett.* **34,** L18804 (2007).
13. Grise, K. M. & Polvani, L. M. The response of midlatitude jets to increased CO_2: distinguishing the roles of sea surface temperature and direct radiative forcing. *Geophys. Res. Lett.* **41,** 2014GL061638 (2014).
14. He, J. & Soden, B. J. Anthropogenic weakening of the tropical circulation: the relative roles of direct CO_2 forcing and sea surface temperature change. *J. Clim.* **28,** 8728–8742 (2015).
15. Bony, S. *et al*. Robust direct effect of carbon dioxide on tropical circulation and regional precipitation. *Nat. Geosci.* **6,** 447–451 (2013).
16. Wu, Y., Seager, R., Ting, M., Naik, N. & Shaw, T. A. Atmospheric circulation response to an instantaneous doubling of carbon dioxide. Part I: model experiments and transient thermal response in the troposphere. *J. Clim.* **25,** 2862–2879 (2012).
17. Wu, Y., Seager, R., Shaw, T. A., Ting, M. & Naik, N. Atmospheric circulation response to an instantaneous doubling of carbon dioxide. Part II: atmospheric transient adjustment and its dynamics. *J. Clim.* **26,** 918–935 (2013).
18. Xie, S.-P. *et al*. Global warming pattern formation: sea surface temperature and rainfall. *J. Clim.* **23,** 966–986 (2010).
19. He, J., Soden, B. J. & Kirtman, B. The robustness of the atmospheric circulation and precipitation response to future anthropogenic surface warming. *Geophys. Res. Lett.* **41,** 2614–2622 (2014).
20. Seager, R., Naik, N. & Vecchi, G. A. Thermodynamic and dynamic mechanisms for large-scale changes in the hydrological cycle in response to global warming. *J. Clim.* **23,** 4651–4668 (2010).
21. Chadwick, R., Good, P., Andrews, T. & Martin, G. Surface warming patterns drive tropical rainfall pattern responses to CO_2 forcing on all timescales. *Geophys. Res. Lett.* **41,** 610–615 (2014).
22. Ackerley, D. & Dommenget, D. Atmosphere-only GCM (ACCESS1. 0) simulations with prescribed land surface temperatures. *Geosci. Model Dev.* **9,** 2077–2098 (2016).
23. Rodwell, M. J. & Hoskins, B. J. Subtropical anticyclones and summer monsoons. *J. Clim.* **14,** 3192–3211 (2001).
24. Giannini, A. Mechanisms of climate change in the semiarid African Sahel: the local view. *J. Clim.* **23,** 743–756 (2010).
25. Chadwick, R. Which aspects of CO_2 forcing and SST warming cause most uncertainty in projections of tropical rainfall change over land and ocean? *J. Clim.* **29,** 2493–2509 (2016).
26. Chavaillaz, Y., Joussaume, S., Bony, S. & Braconnot, P. Spatial stabilization and intensification of moistening and drying rate patterns under future climate change. *Clim. Dynam.* **47,** 951–965 (2016).

Acknowledgements

We thank I. Held, T. Knutson, J. Scheff and L. Polvani for useful discussions. Thanks also go to T. Delworth and K. van der Wiel for their internal review at the Geophysical Fluid Dynamics Laboratory. We acknowledge the World Climate Research Programme's Working Group on Coupled Modeling, which is responsible for CMIP, and we thank the climate modelling groups for producing and making available their model output. J.H. is supported by the Visiting Scientist Program at the department of Atmospheric and Oceanic Science, Princeton University.

Author contributions

J.H. designed the research and analysed the simulations. J.H. and B.J.S. discussed the results. J.H. led the writing with the assistance of B.J.S.

Additional information

Supplementary information is available in the online version of the paper. Reprints and permissions information is available online at www.nature.com/reprints. Correspondence and requests for materials should be addressed to J.H.

Competing financial interests

The authors declare no competing financial interests.

Methods

Model simulations. We use the monthly mean output from a suite of Coupled Model Intercomparison Project Phase 5 (CMIP5) experiments. They include coupled experiments forced with abrupt CO_2 quadrupling (abrupt4×CO_2) and 1% per year CO_2 increase (1pctCO_2). They also include fixed-SST atmospheric general circulation model experiments forced with 4×CO_2 (AMIP_CO_2), 4K uniform SST warming (AMIP_mean) and structured SST warming taken as the CMIP3 ensemble mean SST changes at 4×CO_2 (AMIP_future). The pattern of SST changes in the 1pctCO_2 and AMIP_future simulations are very similar to each other (Supplementary Section 7). In all of the AMIP simulations, land is fully coupled with the atmosphere, and no change in sea ice is prescribed. Finally, we use fixed-SST aquaplanet experiments forced with 4×CO_2 (aqua_CO_2) and 4K uniform SST warming (aqua_mean). Detailed description about these experiments can be found in http://cmip-pcmdi.llnl.gov/cmip5/docs/Taylor_CMIP5_dec31.pdf.

We use all of the models that currently provide all of the variables analysed in this paper, which include 13 models for the abrupt4×CO_2 simulation: bcc-csm1-1, CanESM2, CNRM-CM5, FGOALS-g2, GISS-E2-H, GISS-E2-R, IPSL-CM5A-LR, IPSL-CM5B-LR, MIROC5, MPI-ESM-LR, MPI-ESM-MR, MRI-CGCM3 and NorESM1-M. Nine models are used for the 1pctCO_2 and AMIP simulations: bcc-csm1-1, CanAM4, CNRM-CM5, HadGEM2-A, IPSL-CM5B-LR, MIROC5, MPI-ESM-LR, MPI-ESM-MR and MRI-CGCM3. Six models are used for the aquaplanet simulations: CCSM4, CNRM-CM5, IPSL-CM5A-LR, MPI-ESM-LR, MPI-ESM-MR and MRI-CGCM3. One realization from each model is taken.

The abrupt4×CO_2 simulation is run for 150 years and climate change is calculated as the deviation from the pre-industrial control run. The 1pctCO_2 simulation is run for 140 years and climate perturbation is calculated as the difference between years 121–140 and years 1–20. The AMIP simulations are run for 30 years, whereas the aquaplanet simulations are run for 5 years.

To ensure that the magnitude of forcing in the fixed-SST experiments matches that in the 1pctCO_2 experiment, climate changes in the AMIP and aquaplanet simulations are first scaled linearly to match the CO_2 and tropical SST forcing in the 1pctCO_2 simulations. Specifically, the changes from the AMIP_CO_2 and aqua_CO_2 simulation are multiplied by a factor of $\ln(3.3)/\ln(4.0)$ to match the CO_2 increase in the 1pctCO_2 simulation (where CO_2 increases by a factor of 3.3 between years 1 and 120); that is, we assume that the climate responds logarithmically to increasing CO_2. Likewise, changes from the AMIP_mean, AMIP_future and aqua_mean simulations are divided by their corresponding tropical mean SST changes and multiplied by the tropical mean SST changes from 1pctCO_2. We subtract AMIP_mean from AMIP_future to get the response from the pattern of SST change (AMIP_pattern). Finally, climate change is normalized by each model's global mean surface temperature change in the 1pctCO_2 simulation, to avoid domination by models with large climate sensitivity.

Definition of the subtropical precipitation decline (SPD) regions. The SPD regions refer to areas between the 10° and 50° latitude, where models project a robust precipitation decline. Robustness is given to regions where the amplitude of the ensemble mean change exceeds one inter-model standard deviation. We validated this definition of robustness by alternatively defining robustness as 85% or more model agreement (8 out of 9 models for 1pctCO_2 and AMIP; 12 out of 13 for abrupt4×CO_2) on the sign of precipitation change, which yields similar results (Supplementary Section 1). The red stippling in Figs 1e,f and 3a,b,d–f marks the SPD regions for the abrupt4×CO_2, the 1pctCO_2 and the sum of the AMIP simulations, which all project similar locations of SPD.

For the aquaplanet simulation, we define the SPD regions as the latitudinal bands between the 10° and 50° latitude where the zonal mean precipitation change from the sum of aqua_CO_2 and aqua_mean is negative. The precipitation responses from the aquaplanet simulations are shown in Supplementary Section 7.

Moisture budget decomposition. We decompose precipitation changes on the basis of the column-integrated moisture budget[20], $\partial P = -\langle\nabla\cdot(V\cdot\partial q)\rangle - \langle\nabla\cdot(\partial V\cdot q)\rangle + \partial E + R$. P, V, q and E are the monthly mean precipitation, horizontal velocity, specific humidity and evaporation, respectively. ∂ denotes the perturbation from the base climate. $\langle^*\rangle$ represents column mass integration from the surface pressure level to 50 hPa, above which moisture is extremely small. If the surface variable is not available, we take it from the lowest pressure level. Here, we neglect the cross-term $-\langle\nabla\cdot(\partial V\cdot\partial q)\rangle$, which is small compared with the other terms. The four terms on the right-hand side represent the thermodynamic precipitation change, the dynamic precipitation change, changes in evaporation and the residual (R). The residual consists mostly of changes in transient eddy transport except over regions of sharp topography and the deep tropics[20].